

# 3D layered-integrated modelling of mass exchange in semi-enclosed water bodies

## Modélisation 3D intégrée par couches de l'échange de masse dans les volumes d'eau semi-fermés

C.W. LI & J. GU, *Department of Civil & Structural Engineering, The Hong Kong Polytechnic University*

### ABSTRACT

The flow patterns in semi-enclosed water bodies are generally complicated and have significant effect on the water quality and fluid exchange there. The exchange of fluid between the semi-enclosed water body and outside is due to two physical mechanisms. The first is the flushing due to tidal effect. The second is the shear induced by the velocity difference between the flow within the water body and outside. To predict the flow and solute transport in these water bodies a three-dimensional layer-integrated numerical model has been developed. To account for the turbulence which consists of the free shear component and the bottom friction component the k- $\epsilon$  model is employed. The numerical model has been applied to the cases of tidal flow as well as steady river flow outside a rectangular harbour with or without breakwater. Compared with the available experimental results, the gross mass exchange both due to tidal effect and shear can be estimated satisfactorily by the numerical model.

### RÉSUMÉ

Les configurations d'écoulement dans les volumes d'eau semi-fermés sont généralement compliquées et ont un effet significatif sur la qualité de l'eau et les échanges de fluides. L'échange de fluide entre la masse d'eau semi-fermée et l'extérieur est dû à deux mécanismes physiques. Le premier est le flot lié à la marée. Le second est le cisaillement induit par la différence de vitesse de l'eau entre l'intérieur et l'extérieur. Pour prévoir l'écoulement et le transport d'effluents dans ces masses d'eau, un modèle tri-dimensionnel numérique intégré par couches a été développé. Pour tenir compte de la turbulence qui comprend la composante de cisaillement libre et le frottement au fond, on utilise le modèle k- $\epsilon$ . Le modèle numérique a été appliqué aussi bien au cas de la marée qu'à celui d'un écoulement permanent de rivière à l'extérieur d'un port rectangulaire avec ou sans brise-lame. Comparé aux résultats expérimentaux disponibles, l'échange de masse brut dû à la marée et à l'écoulement cisailé, donné par le modèle numérique, peut être considéré comme satisfaisant.

### Introduction

Harbors, typhoon shelters, and marina are semi-enclosed water bodies with breakwaters constructed. They are designed and constructed for the protection of the users from storm and flood waves. Although wave protection has generally been the primary objectives in the design layout, the exchange of mass in the water body with the external flow should also be the significant factors influencing the design layout, particularly with regard to the water quality as well as sediment deposition considerations.

One important parameter affecting the water quality and sediment deposition process is the residence time which is defined as the ratio between the average flux of water leaving the water body and the volume of the water body. For basins situated in rivers, performing a mass balance analysis for the enclosed water body, we can show that

$$\frac{D(\bar{c}V)}{Dt} = -q(c - c_a) \quad (1)$$

where  $\bar{c}$  = average concentration of a solute in the water body,  $V$  = volume of the water body,  $q$  = average volume flux leaving the water body,  $c$  = average concentration at the entrance of the water body,  $c_a$  = background concentration. If the solute is well mixed within the water body (i.e.  $c = \bar{c}$ ) and all the parameters have constant values, the solution of equation (1) is given by

$$\frac{\bar{c} - c_a}{c_0 - c_a} = \exp\left(-\frac{t}{\tau}\right) \quad (2)$$

where  $\tau = q/V$  = residence time, or retention time, according to Booji (1986) and Anestis & Chu (1985);  $c_0$  = initial concentration within the water body.

In the presence of tide, the major flushing mechanism is the rise and fall of the water level. The mass balance equation becomes (e.g. Sanford, et al., 1992)

$$\frac{D(\bar{c}V)}{Dt} = -(1-b)Q(\bar{c} - c_a) \quad (3)$$

where  $b$  = return flow factor = fraction of water leaving during ebb that returns during flood;  $0 < b < 1$ ; and  $Q = P/T$ ,  $P$  = tidal prism =  $A_s R$ ,  $A_s$  = surface area,  $R$  = tidal range,  $T$  = tidal period. The solution can also be expressed by equation (2), with

$$\tau = \frac{V}{(1-b)Q} = \frac{VT}{(1-b)P} \quad (4)$$

The problem remained is on the determination of the return factor  $b$  which is dependent on the fate of the plume of the effluent water.

In both cases turbulence will be important for the determination of the mass exchange process. The parameters  $q$  and  $b$  are highly dependent on the turbulent nature of the flow. The complicated flow pattern may also affect the well-mixed condition used above. Due to the presence of bottom friction, and occasionally wind forcing and density stratification, the flow field is three-dimensional. To avoid empirical estimation of the dispersion terms arising from depth-integration and to predict more accurately the velocity field and flushing efficiency of these semi-enclosed water

Revision received June 23, 2000. Open for discussion till February 28, 2002.

bodies three-dimensional model is required.

For the closure approximation of the effective stresses, many turbulent models have been developed. The most commonly used model in engineering applications is the two-equation models, including the k-ε model and k-ω model (e.g. Wilcox, 1993). Li et al. (1997) demonstrated that these two models have similar accuracy when being applied to free surface recirculating flow subjected to bottom friction. It has been pointed out that the anisotropic nature of turbulence in such type of shallow water flow will cause an underestimation of the horizontal eddy viscosity by the k-ε model (Bijvelds et al., 1999).

In the present work a layer-integrated three-dimensional model is developed for the simulation of tidal flow and solute transport in semi-enclosed water bodies. The turbulent Reynolds stresses are parameterised by the k-ε model. The reason of choosing the k-ε model is that it is the most commonly used model and has been applied to many cases of engineering applications. Before proposing any modification to the k-ε model its performance should be assessed first. For the numerical algorithm an operator splitting method is used so that different numerical schemes can be used to approximate different physical processes. The governing equations are split into three parts in the solution: advection, dispersion and propagation. In the advection part the advective accelerations are approximated by the four-node minimax-characteristics method (Li, 1990). In the dispersion step the diffusive terms are solved by the central difference method. In the propagation step the surface elevation (pressure) is obtained from the solution of the Poisson type equation. The model is tested against laboratory measurements for different type of flows and boundary conditions.

## 2. Governing equations

By assuming hydrostatic pressure and neglecting the vertical velocity and the effects of wind and Coriolis force, the quasi-three-dimensional layer-integrated equations of motion are written as:

$$\frac{\partial q_{kx}}{\partial t} + U_k \frac{\partial q_{kx}}{\partial x} + V_k \frac{\partial q_{kx}}{\partial y} = \frac{\partial}{\partial x} (2h_k v_k \frac{\partial U_k}{\partial x}) + \frac{\partial}{\partial y} (h_k v_k \frac{\partial U_k}{\partial y}) + \frac{\partial}{\partial y} (h_k v_k \frac{\partial V_k}{\partial x}) + h_k \frac{\partial}{\partial z} (v_k \frac{\partial U_k}{\partial z}) - gh_k \frac{\partial \eta}{\partial x} + \left[ \frac{\partial}{\partial x} \int_{h_k} (U_k - \bar{U}_k)^2 dz + \frac{\partial}{\partial y} \int_{h_k} (U_k - \bar{U}_k)(V_k - \bar{V}_k) dz \right] \quad (5)$$

$$\frac{\partial q_{ky}}{\partial t} + U_k \frac{\partial q_{ky}}{\partial x} + V_k \frac{\partial q_{ky}}{\partial y} = \frac{\partial}{\partial x} (2h_k v_k \frac{\partial U_k}{\partial y}) + \frac{\partial}{\partial x} (h_k v_k \frac{\partial V_k}{\partial x}) + \frac{\partial}{\partial y} (h_k v_k \frac{\partial V_k}{\partial y}) + h_k \frac{\partial}{\partial z} (v_k \frac{\partial U_k}{\partial z}) - gh_k \frac{\partial \eta}{\partial y} + \left[ \frac{\partial}{\partial y} \int_{h_k} (V_k - \bar{V}_k)^2 dz + \frac{\partial}{\partial x} \int_{h_k} (U_k - \bar{U}_k)(V_k - \bar{V}_k) dz \right] \quad (6)$$

and the continuity equation is:

$$\frac{\partial \eta}{\partial t} + \sum_{k=1}^n \left( \frac{\partial q_{kx}}{\partial x} + \frac{\partial q_{ky}}{\partial y} \right) = 0 \quad (7)$$

The mass conservation of solute is:

$$\frac{\partial h_k C_k}{\partial t} + U_k \frac{\partial h_k C_k}{\partial x} + V_k \frac{\partial h_k C_k}{\partial y} = \frac{\partial}{\partial x} \left( \frac{h_k v_k}{\sigma_t} \frac{\partial C_k}{\partial x} \right) + \frac{\partial}{\partial y} \left( \frac{h_k v_k}{\sigma_t} \frac{\partial U_k}{\partial y} \right) + \frac{\partial}{\partial y} \left( \frac{h_k v_k}{\sigma_t} \frac{\partial V_k}{\partial x} \right) + h_k \frac{\partial}{\partial z} \left( \frac{v_k}{\sigma_t} \frac{\partial U_k}{\partial z} \right) + \left[ \frac{\partial}{\partial x} \int_{h_k} (U_k - \bar{U}_k)(C_k - \bar{C}_k) dz + \frac{\partial}{\partial y} \int_{h_k} (V_k - \bar{V}_k)(C_k - \bar{C}_k) dz \right] \quad (8)$$

where x = longitudinal co-ordinate direction; y = transverse co-ordinate direction; z = vertical co-ordinate direction;  $U_k$  = longitudinal velocity in layer k;  $V_k$  = transverse velocity in layer k;  $h_k$  = thickness of layer k; N = total number of layers;  $\eta$  = free surface elevation;  $v_k$  = eddy viscosity in layer k;  $q$  = longitudinal flow rate in layer k;  $q_{kx}$  = transverse flow rate in layer k;  $g$  = acceleration due to gravity;  $C_k$  = solute concentration in layer k;  $\sigma_t$  = turbulent Schmidt number. The interaction between each layer is through vertical diffusion. The friction terms are introduced as surface and bottom boundary conditions.

The last terms in equations (5), (6) and (8) are called momentum dispersion terms. These terms are due to vertical non-uniformity of the mean flow quantities in every layer. When the water flow is simulated by depth-averaged model, the vertical non-uniformity of the mean-flow quantities may be large and cannot be neglected. However, when the flow is simulated by layer-integrated model, U and V are almost uniform in every layer and thus the momentum dispersion terms become very small and can be neglected. The eddy viscosity  $\nu$  appearing in equation (1) and (2) is given by:

$$v_k = C_\mu \frac{k_k^2}{\epsilon_k} \quad (9)$$

where:  $k$  = turbulence kinetic energy of layer k;  $\epsilon$  = turbulence dissipation of layer k. The k-equation is:

$$\frac{\partial k_k}{\partial t} + U_k \frac{\partial k_k}{\partial x} + V_k \frac{\partial k_k}{\partial y} = \frac{\partial}{\partial x} \left( \frac{v_k}{\sigma_k} \frac{\partial k_k}{\partial x} \right) + \frac{\partial}{\partial y} \left( \frac{v_k}{\sigma_k} \frac{\partial k_k}{\partial y} \right) + \frac{\partial}{\partial z} \left( \frac{v_k}{\sigma_k} \frac{\partial k_k}{\partial z} \right) - \epsilon_k + v_k \left[ 2 \left( \frac{\partial U_k}{\partial x} \right)^2 + 2 \left( \frac{\partial V_k}{\partial y} \right)^2 + \left( \frac{\partial U_k}{\partial z} \right)^2 + \left( \frac{\partial V_k}{\partial z} \right)^2 + \left( \frac{\partial U_k}{\partial y} + \frac{\partial V_k}{\partial x} \right)^2 \right] \quad (10)$$

The ε-equation is:

$$\begin{aligned} \frac{\partial \varepsilon_k}{\partial t} + U_k \frac{\partial \varepsilon_k}{\partial x} + V_k \frac{\partial \varepsilon_k}{\partial y} &= \frac{\partial}{\partial x} \left( \frac{v_k}{\sigma_\varepsilon} \frac{\partial \varepsilon_k}{\partial x} \right) + \frac{\partial}{\partial y} \left( \frac{v_k}{\sigma_\varepsilon} \frac{\partial \varepsilon_k}{\partial y} \right) \\ &+ \frac{\partial}{\partial z} \left( \frac{v_k}{\sigma_\varepsilon} \frac{\partial \varepsilon_k}{\partial z} \right) - C_{2\varepsilon} \frac{\varepsilon_k^2}{k_k} + C_{1\varepsilon} \frac{\varepsilon_k}{k_k} v_k \left[ 2 \left( \frac{\partial U_k}{\partial x} \right)^2 \right. \\ &\left. + 2 \left( \frac{\partial V_k}{\partial y} \right)^2 + \left( \frac{\partial U_k}{\partial z} \right)^2 + \left( \frac{\partial V_k}{\partial z} \right)^2 + \left( \frac{\partial U_k}{\partial y} + \frac{\partial V_k}{\partial x} \right)^2 \right] \end{aligned} \quad (11)$$

where  $C_{\mu} = 0.09$ ,  $C_{1\varepsilon} = 1.44$ ,  $C_{2\varepsilon} = 1.92$ ,  $\sigma_k = 1.0$  and  $\sigma_\varepsilon = 1.3$  as recommended by Launder and Spalding (1974).

### 3. Numerical scheme

The split-operator approach is used in the solution of the governing equations. At each time step, the equations are split into three steps: Advection, Diffusion and Propagation & Source terms. The equations for the Advection step are:

$$\frac{q_{kx}^{n+1/3} - q_{kx}^n}{\Delta t} + U_k \frac{\partial q_{kx}}{\partial x} + V_k \frac{\partial q_{kx}}{\partial y} = 0 \quad (12)$$

$$\frac{q_{ky}^{n+1/3} - q_{ky}^n}{\Delta t} + U_k \frac{\partial q_{ky}}{\partial x} + V_k \frac{\partial q_{ky}}{\partial y} = 0 \quad (13)$$

$$\frac{\Phi_{ky}^{n+1/3} - \Phi_{ky}^n}{\Delta t} + U_k \frac{\partial \Phi_{ky}}{\partial x} + V_k \frac{\partial \Phi_{ky}}{\partial y} = 0 \quad (14)$$

$$\frac{k_k^{n+1/3} - k_k^n}{\Delta t} + U_k \frac{\partial k_k}{\partial x} + V_k \frac{\partial k_k}{\partial y} = 0 \quad (15)$$

$$\frac{\varepsilon_k^{n+1/3} - \varepsilon_k^n}{\Delta t} + U_k \frac{\partial \varepsilon_k}{\partial x} + V_k \frac{\partial \varepsilon_k}{\partial y} = 0 \quad (16)$$

where  $\Phi_k = h_k C_k$ . The four-node Minimax-Characteristics scheme (Li, 1990) is used to solve the equations of pure advection. The equations for the diffusion step are:

$$\frac{q_{kx}^{n+2/3} - q_{kx}^{n+1/3}}{\Delta t} = \frac{\partial}{\partial x} (2h_k v_k \frac{\partial U_k}{\partial x}) + \frac{\partial}{\partial y} (h_k v_k \frac{\partial U_k}{\partial y}) + \frac{\partial}{\partial z} (h_k v_k \frac{\partial U_k}{\partial z}) \quad (17)$$

$$\frac{q_{ky}^{n+2/3} - q_{ky}^{n+1/3}}{\Delta t} = \frac{\partial}{\partial x} (2h_k v_k \frac{\partial U_k}{\partial y}) + \frac{\partial}{\partial y} (h_k v_k \frac{\partial V_k}{\partial x}) + \frac{\partial}{\partial z} (h_k v_k \frac{\partial U_k}{\partial z}) \quad (18)$$

$$\frac{\Phi_k^{n+1} - \Phi_k^{n+1/3}}{\Delta t} = \frac{\partial}{\partial x} \left( \frac{v_k}{\sigma_k} \frac{\partial \Phi_k}{\partial x} \right) + \frac{\partial}{\partial y} \left( \frac{v_k}{\sigma_k} \frac{\partial \Phi_k}{\partial y} \right) + \frac{\partial}{\partial z} \left( \frac{v_k}{\sigma_k} \frac{\partial \Phi_k}{\partial z} \right) \quad (19)$$

$$\frac{k_k^{n+2/3} - k_k^{n+1/3}}{\Delta t} = \frac{\partial}{\partial x} \left( \frac{v_k}{\sigma_k} \frac{\partial k_k}{\partial x} \right) + \frac{\partial}{\partial y} \left( \frac{v_k}{\sigma_k} \frac{\partial k_k}{\partial y} \right) + \frac{\partial}{\partial z} \left( \frac{v_k}{\sigma_k} \frac{\partial k_k}{\partial z} \right) \quad (20)$$

$$\frac{\varepsilon_k^{n+2/3} - \varepsilon_k^{n+1/3}}{\Delta t} = \frac{\partial}{\partial x} \left( \frac{v_k}{\sigma_\varepsilon} \frac{\partial \varepsilon_k}{\partial x} \right) + \frac{\partial}{\partial y} \left( \frac{v_k}{\sigma_\varepsilon} \frac{\partial \varepsilon_k}{\partial y} \right) + \frac{\partial}{\partial z} \left( \frac{v_k}{\sigma_\varepsilon} \frac{\partial \varepsilon_k}{\partial z} \right) \quad (21)$$

In the diffusion step, the simple four-node central space scheme is used because the diffusion terms are generally small in horizontal flows. The equations for the Propagation & Source Terms Step are:

$$\frac{\eta^{n+1} - \eta^n}{\Delta t} = - \sum_1^n \left( \frac{\partial q_{kx}}{\partial x} + \frac{\partial q_{ky}}{\partial y} \right) \quad (22)$$

$$\frac{q_{kx}^{n+1} - q_{kx}^{n+2/3}}{\Delta t} = -gh_k \frac{\partial \eta}{\partial x} \quad (23)$$

$$\frac{q_{ky}^{n+1} - q_{ky}^{n+2/3}}{\Delta t} = -gh_k \frac{\partial \eta}{\partial y} \quad (24)$$

$$\frac{k_k^{n+1} - k_k^{n+2/3}}{\Delta t} = v_k \left[ 2 \left( \frac{\partial U_k}{\partial x} \right)^2 + 2 \left( \frac{\partial V_k}{\partial y} \right)^2 + \left( \frac{\partial U_k}{\partial z} \right)^2 + \left( \frac{\partial V_k}{\partial z} \right)^2 + \left( \frac{\partial U_k}{\partial y} + \frac{\partial V_k}{\partial x} \right)^2 \right] - \varepsilon_k \quad (25)$$

$$\frac{\varepsilon_k^{n+1} - \varepsilon_k^{n+2/3}}{\Delta t} = C_{1\varepsilon} \frac{\varepsilon_k}{k_k} v_k \left[ 2 \left( \frac{\partial U_k}{\partial x} \right)^2 + 2 \left( \frac{\partial V_k}{\partial y} \right)^2 + \left( \frac{\partial U_k}{\partial z} \right)^2 + \left( \frac{\partial V_k}{\partial z} \right)^2 + \left( \frac{\partial U_k}{\partial y} + \frac{\partial V_k}{\partial x} \right)^2 \right] - C_{2\varepsilon} \frac{\varepsilon_k^2}{k_k} \quad (26)$$

Equations(22),(23),(24) are solved implicitly and an explicit scheme is employed to solve the equations (25),(26). The three equations (22)~(24) are decoupled through two procedures: First, the unknown flow rates at time lever n+1 are eliminated by differentiating equation (23) with respect to x, and equation (24) with respect to y; Second, the resulting Poisson type equation for  $\eta$  with essential boundary condition is solved by using the Gauss-Seidel iteration method.

Variable rectilinear grid is allowed in the model, i.e.  $\Delta x = f(x)$ ,  $\Delta y = g(y)$ ,  $\Delta z = h(z)$ , where  $\Delta x$ ,  $\Delta y$ ,  $\Delta z$  are grid size in x, y, z directions respectively, and f,g,h are continuous functions. The advantage of using variable grid is that very small grid size can be used at the region in which the velocity variation is large, such as the wall region and the boundary layer separation zone. In the present work, the hyperbolic tangent function is used in all the three directions. To divide a line segment of length L into N sub-segments, with more nodes at the two ends of the line segment, the ordinates of the nodes with origin at one end of the line segment are given by

$$x_i = 0.5 \left( 1 + \frac{\tanh(\delta_i \beta)}{\tanh(\beta)} \right) L \quad (27)$$

$$\delta_i = \frac{2i}{N} - 1 \quad i=0,1,2,\dots,N$$

where  $\beta (>0)$  is a parameter used for the adjustment of the separation between the points.

#### 4. Boundary conditions

At inflow boundary, the vertical variation of the longitudinal velocity  $U$  is specified as a logarithmic profile with a Manning coefficient  $n$  and the transverse velocity  $V$  are assumed equal to zero and all other quantities, i.e, water depth, concentration,  $k$  and  $\epsilon$  are extrapolated from the interior points (zero gradients). Specifically, the inflow velocity is given by

$$U(0, y, z) = \bar{U} + \frac{u_*}{\kappa} \left[ 1 + \ln \left( \frac{z}{H} \right) \right] \quad (28)$$

where  $\bar{U}$  = mean velocity,  $u_*$  = bottom shear velocity,  $H$  = total water depth,  $\kappa$  = von Karman's constant; and

$$u_* = \sqrt{gHs} = \sqrt{\frac{gn^2}{H^{1/3}}} \bar{U} \quad (29)$$

by the Manning equation, where  $n$  = Manning's coefficient,  $s$  = energy slope.

For tidal inflow boundary the time dependent water elevation is specified. The inflow velocity can be computed from the governing equations after solving the Poisson equation for water elevation. At outflow boundary the water depth is determined from a radiation boundary condition (Zhu & Li, 1993) and the velocities, solute concentration,  $k$  and  $\epsilon$  are extrapolated from the interior points (zero gradients).

At solid wall boundary, no-slip boundary condition is used and the wall function technique is applied. At the top layer,  $k$  and  $\epsilon$  are assumed to be very small, approximately zero. The surface stresses  $\tau_{sx}$  and  $\tau_{sy}$  are set to zero. At the bottom layer, the magnitudes of bottom stresses  $\tau_{bx}$  and  $\tau_{by}$  are specified by the Manning equation and the values of  $k$  and  $\epsilon$  at the grid points next to the bottom  $k_b$  and  $\epsilon_b$  are determined by using the law of the wall (e.g. Wilcox, 1993). The normal gradient of the solute concentration is set to zero for solid boundary.

The bottom stresses specifies the bottom boundary conditions for the model

$$v \frac{\partial U}{\partial z} \Big|_{z=0} = \frac{\tau_{bx}}{\rho}; v \frac{\partial V}{\partial z} \Big|_{z=0} = \frac{\tau_{by}}{\rho} \quad (30)$$

and they are given by the quadratic law

$$\frac{\tau_b}{\rho} = u_*^2 = \frac{gn^2}{H^{1/3}} (\bar{U}^2 + \bar{V}^2) \quad (31)$$

from (29), also

$$\frac{\tau_{bx}}{\rho} = \frac{gn^2}{H^{1/3}} \bar{U} (\bar{U}^2 + \bar{V}^2)^{1/2}; \frac{\tau_{by}}{\rho} = \frac{gn^2}{H^{1/3}} \bar{V} (\bar{U}^2 + \bar{V}^2)^{1/2} \quad (32)$$

#### 5. Model verification

Before application of the numerical model to real harbour with complicated shape and variable bottom topography, the model should be validated by simple cases in which experimental data are available. The model has been successfully applied to cases of recirculating flow (Li & Yu, 1996) with the standard  $k$ - $\epsilon$  model of turbulence and to cases of tidal flow in rectangular harbour with the  $k$ - $\omega$  model of turbulence (Li & Zhang, 1998). The present work will concentrate on the mass exchange process.

##### *Mass exchange in a rectangular harbour with steady flow outside*

For harbour adjacent to river the exchange of mass is dominated by the shear due to the velocity difference between the river flow and the flow inside the harbour. In addition a breakwater will normally be built at the harbour entrance to reduce the impact due to the flow from the river. In small harbours in which the mixing can be assumed complete, the mass flux leaving the harbour can be related to the concentration inside the harbour and velocity in the river. Equation (2) can be rewritten as

$$c = c_0 \exp\left(-\frac{ku_a A}{V} t\right) \quad (33)$$

where  $q = ku_a A$ ;  $u_a$  = velocity in the river,  $A$  = sectional area of the harbour entrance;  $k$  = a coefficient which is expected to be a constant.

Due to the complication in the flow patterns at the harbour entrance, the coefficient  $k$  can have a range of values. Booij (1986) obtained a value about 0.032 for physical model harbours with vertical sidewalls. Altai and Chu (1997) obtained two average values of  $k$ , one is 0.022 if the turbulence exchange is in an active mode of oscillation, and the other is 0.013 if the turbulence exchange is in a passive mode of coexistence with the flow in the harbour. Van Schijndel and Kranenburg (1998) obtained a significantly lower value of 0.0018 in a physical model of the harbour named 'Het Steel'.

Li and Yip (1999) obtained a value of 0.03 for physical model harbours with narrow entrances if there is only one gyre in the harbour. A smaller value of 0.016 is obtained for the basin with large aspect ratio and narrow entrance. In this case the flow pattern consists of at least two gyres, with one gyre at the innermost part of the basin. This causes a nonuniform distribution of the concentration within the harbour (i.e. the well-mixed condition is not achieved) and resulting in a significant increase in residence time.

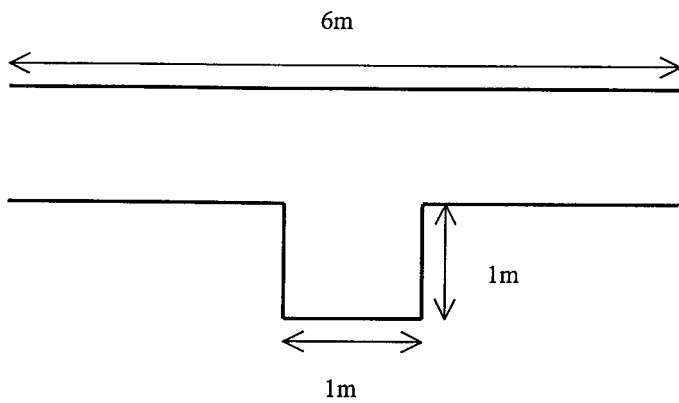


Fig. 1. Schematic layout of the model river-harbour system.

The numerical model was set up to replicate the laboratory conditions. The model domain covered the model harbour of horizontal dimension 1m x 1m and the main flow region beyond the harbour entrance (Fig.1). The water depth is 0.1m. Nonuniform grid is used so that the boundary layer separation at the tip of the harbour can be simulated. The smallest grid size used is 1.5cm which is just 1.5% of the harbour size. The Manning's n of 0.015 is used. For the open boundary conditions, a uniform mean velocity of

0.1m/s is specified. The numerical model was always started from 'cold' – zero initial condition. The flow attains a steady state in about 50s. Solute is then added into the harbour uniformly by assigning a value of 1 to the concentration nodes within the harbour. The computation continues and the temporal variation of the concentration is then obtained. Fig. 2 displays a snapshot of the velocity field together with the concentration field. Fig. 3 displays the temporal variation of the spatially averaged concentration within the harbour. The coefficient k derived from the computed results is approximately 0.03, which is in the high side of the experimentally obtained data range.

It is observed that the effect of grid size near the boundary separation region is quite significant for the determination of the mass exchange rate. Using a uniform grid size 5cm the coefficient k obtained is only 0.015, which is in the lower range of the measured values (Fig. 3). This is obvious as the use of coarse grid will underestimate the velocity gradient and lead to the underestimation of the mass exchange which is mainly due to the shear layer at the harbour entrance.

As the experimentally measured value of k has a range of variation (0.013-0.032 for the case with one gyre in the harbour), the uncertainty induced by the numerical model for its inability to

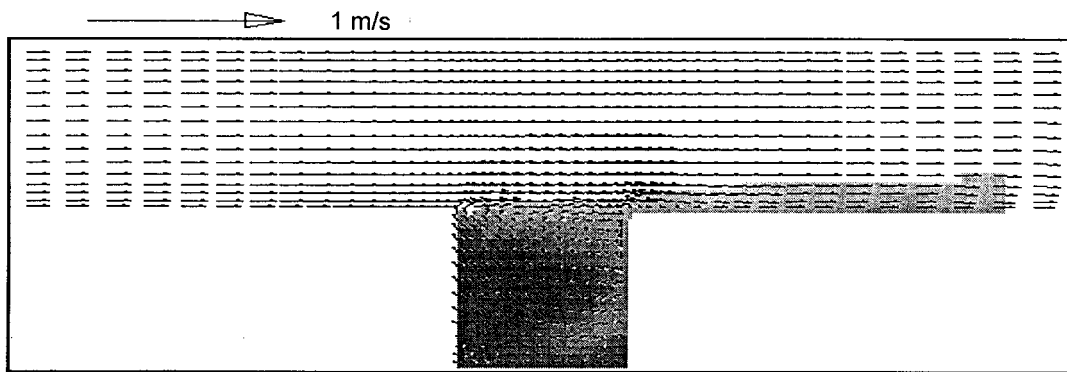


Fig. 2. Typical flow field and concentration distribution in the river-harbour system.

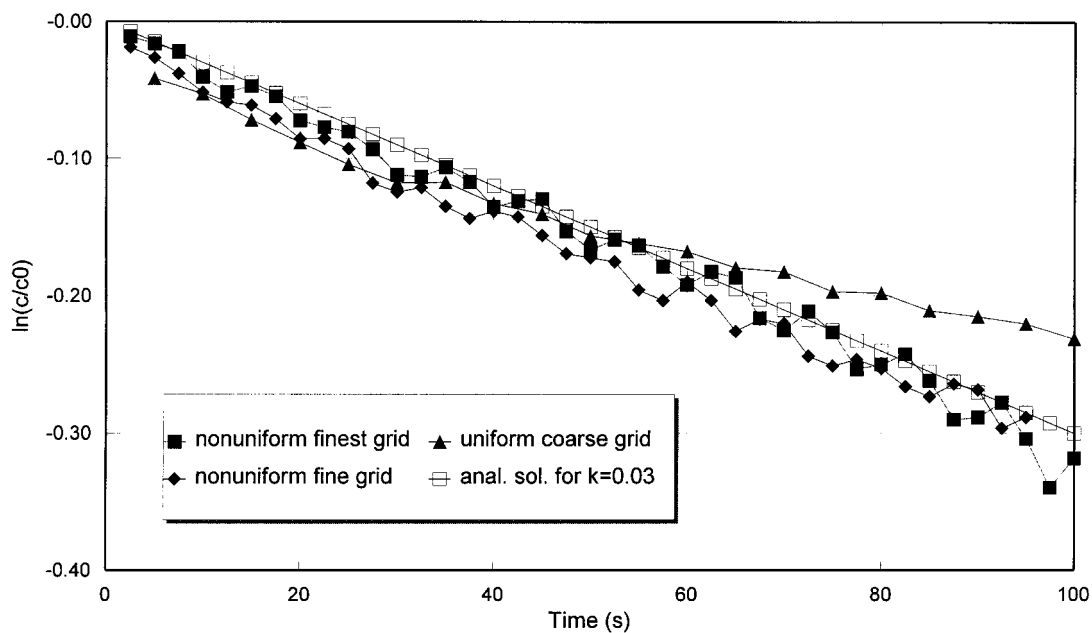


Fig. 3. Temporal variation of the average concentration within the harbour.

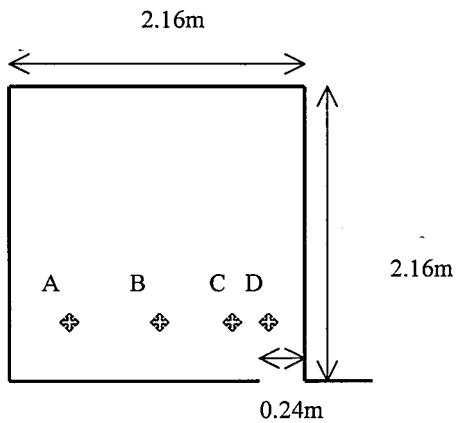


Fig. 4. Schematic layout of the tidal harbour with output points.

simulate anisotropic turbulence may not be assessed based on the comparison between the computed and experimentally determined results. However, it is suspected that the uncertainty is not significant as the mass exchange at the harbour entrance is dominated by horizontal shear, and bottom friction only plays a minor role.

#### Tidal flushing in a square harbour

For harbour with narrow entrance and subjected to tidal motion, the flow entering the harbour during flood will be jet-like and recirculating flow will result. Experimental measurements of tide-

induced circulation in a laboratory harbour were done by Nece & Falconer (1989), Falconer & Yu (1990). The numerical model was set up to replicate the laboratory conditions (Fig. 4). The model domain covered the model harbour and a large region beyond the harbour entrance. Based on the results of the calibration tests, the Manning's  $n$  of 0.01 is used. For the open boundary conditions, a sinusoidal tide of period 1416s was specified at the open boundary parallel to the plane of the harbour entrance. For the two open boundaries perpendicular to the harbour entrance plane, the boundaries were assumed to be free slip boundaries giving rise to a zero lateral velocity gradient along these boundaries. For the closed boundaries, the law of the wall is used. The tidal range is 100mm and the water depth is 150mm. The numerical model was always started from a state of rest at low tide.

The exchange characteristics of the model harbour can be determined by filling the water body by a tracer of constant concentration initially, and then monitoring the concentration variation within the water body. By defining the exchange coefficient as the fraction of water in the basin at high water slack which is flushed out from the basin and replaced by ambient water during the cycle ending at the next high water slack, the equation for it is given by

$$E = 1 - \left( \frac{C_i}{C_0} \right)^i \quad (34)$$

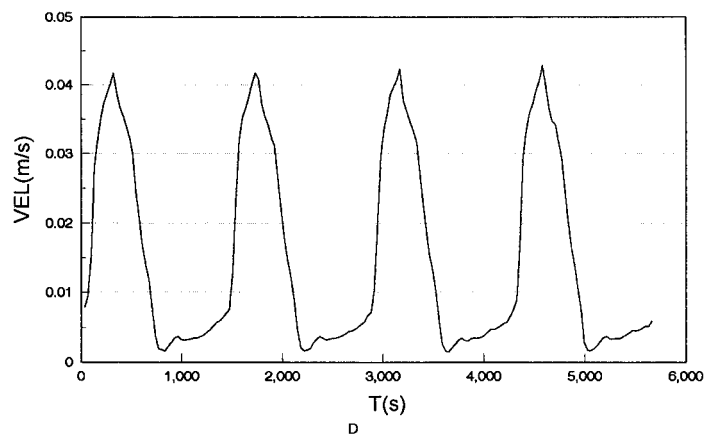
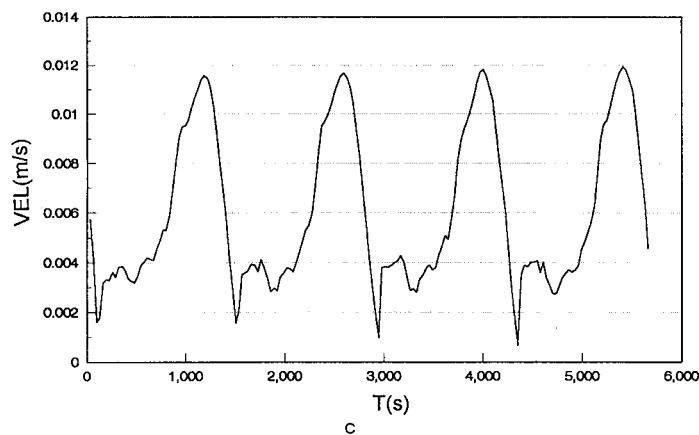
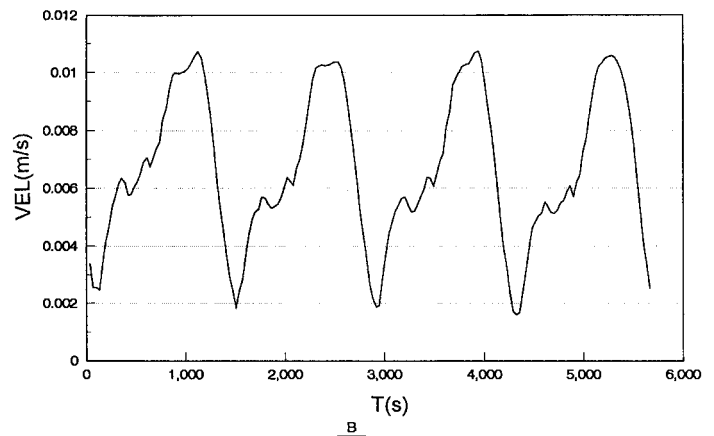
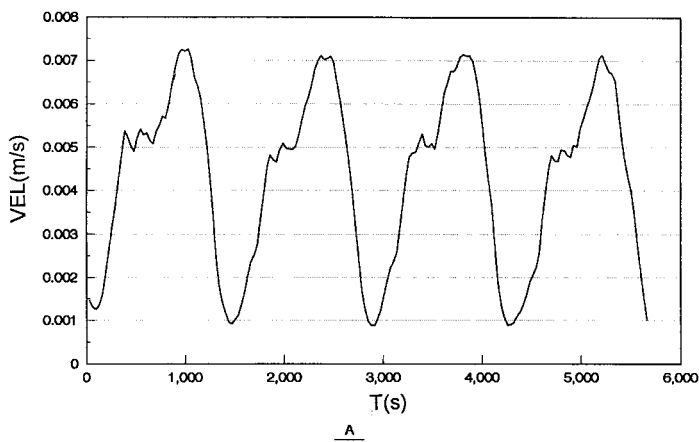


Fig. 5. Temporal variation of the depth-averaged velocity at points A,B,C,D.

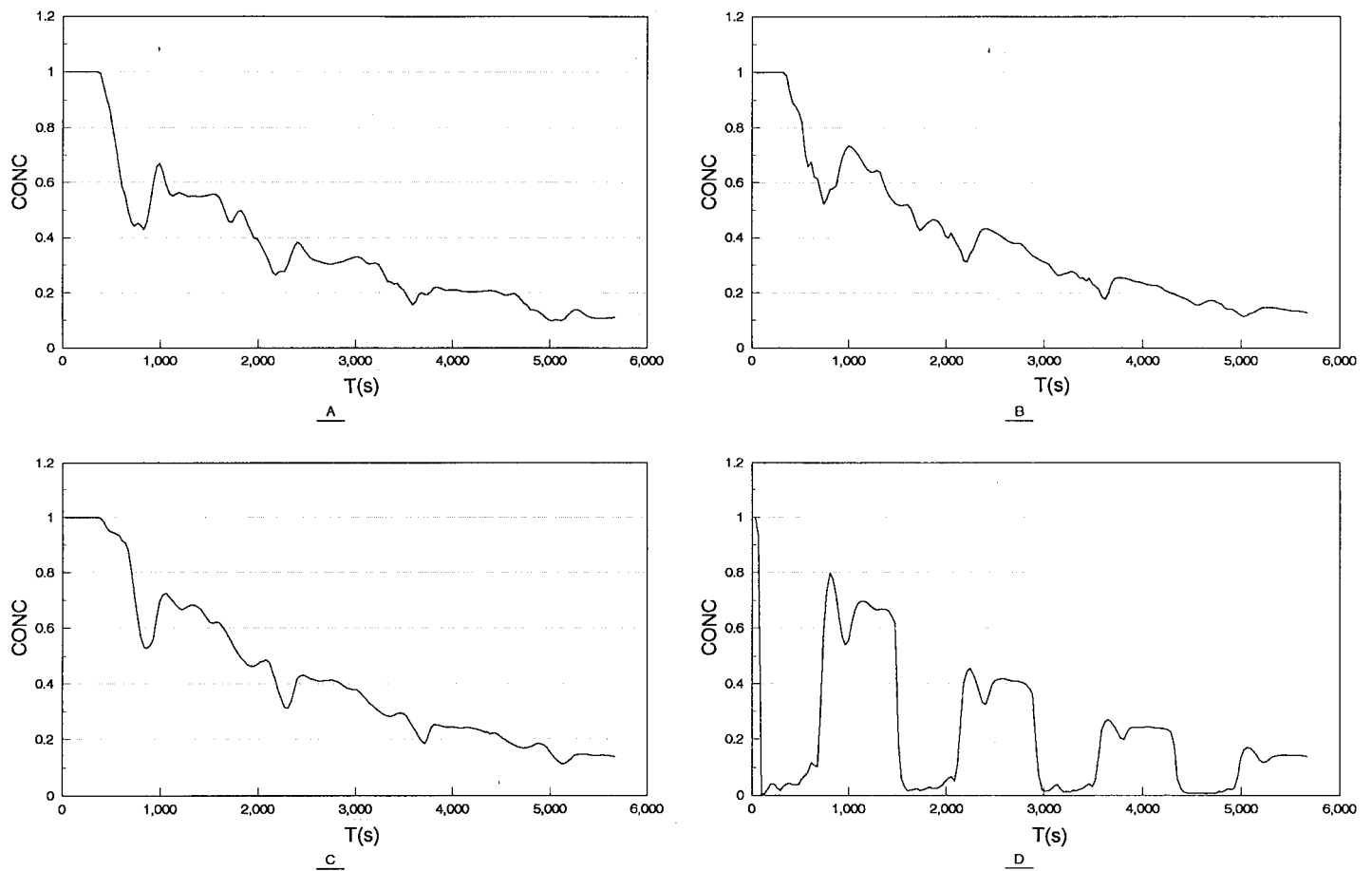


Fig. 6. Temporal variation of the depth-averaged concentration at points A,B,C,D.

where  $E$  = average per cycle exchange coefficient,  $C_0$  = initial spatially averaged concentration and  $C_i$  = final spatially averaged concentration after  $i$  tidal cycles. Comparing with equation (3), we get

$$E = 1 - [\exp(-iP(1-b)/V)]^{1/i} \quad (35)$$

In the numerical model the initial concentration of a tracer is set to 1 in the harbour, and zero elsewhere. The temporal variation of

the velocity and concentration due to tidal action are then computed. Fig. 4 indicates the locations of the points for which the temporal variation of the depth-averaged velocity and depth-averaged concentration are output. The temporal variation of velocity and concentration at 4 locations A,B,C,D are displayed (Figs. 5&6). The periodic variation of the velocities due to tidal effect is clearly observed. The periodic variation of the concentration are not so significant. It is most obvious at point A through which the fresh water is transported. The exchange coefficient displays

Measured					Simulated				
0.445	0.448	0.450	0.448	0.449	0.471	0.464	0.475	0.477	0.453
0.440	0.445	0.444	0.446	0.447	0.442	0.410	0.460	0.391	0.383
0.436	0.426	0.408	0.415	0.421	0.437	0.406	0.425	0.384	0.383
0.428	0.432	0.366	0.406	0.416	0.444	0.406	0.409	0.389	0.385
0.397	0.404	0.370	0.392	0.415	0.428	0.432	0.418	0.408	0.405

Fig. 7. Computed and measured exchange coefficients at various points.

a spatial variation after four tidal cycles, showing that the well-mixed condition has not been achieved. The average exchange coefficient in the harbour is obtained by spatially averaging the concentration in the harbour at the end after four tidal cycles. The value obtained is 0.425, which is very close to the experimentally determined value of 0.424 (Falconer & Yu, 1990). The point to point comparison of the exchange coefficient exhibits a difference which is around  $\pm 10\%$  (Fig. 7). As the concentration is highly transient and with large spatial variation, the point to point comparison can easily have error. Another source of discrepancy is that the flow may not be fully turbulent everywhere.

## 6. Conclusions

A three-dimensional layer-integrated numerical model has been developed and applied to study mass exchange in semi-enclosed water bodies. The model includes the  $k$ - $\epsilon$  equations of turbulence and allows variable rectilinear grid. The empirical estimation of diffusion coefficients is thus avoided. In determining the complicated tide induced and shear induced mixing phenomena in semi-enclosed water bodies, the numerical model produces results that fall within the experimentally measured range.

## Acknowledgements

This work was supported by a grant from the Research Grant Council of the Hong Kong Special Administrative Region (Project No. HKP40/94E) and a grant from the Area of Strategic Development Scheme in Hydraulics, the Hong Kong Polytechnic University.

## References

ALTAI, W. and CHU, V.H. (1997) 'Retention time in recirculating flow', Proc. 27<sup>th</sup> Congress of IAHR, theme B, vol. 1, pp. 9-15.

ANESTIS, I.D. and CHU, V.H. (1985) 'Entrapment characteristics in a recirculating eddies', Proc. 21<sup>st</sup> Congress of IAHR, vol. 2, pp. 7-11.

BIJVELDS, M.D.J.P., KRANENBURG, C., and STELLING, G.S., (1999) '3D numerical simulation of turbulent shallow-water flow in square harbour', Journal of Hydraulic Engrg., ASCE, 125, 1, pp. 26-31.

BOOJI, R., (1986) 'Exchange of mass in harbours', Proc. 23<sup>rd</sup> Congress of IAHR, Ottawa, vol. D, pp. 69-74

FALCONER, R.A. and YU, G.P., (1990) 'Effect of depth, bed slope and scaling on tidal currents and exchange in a laboratory model harbour', Proc. Inst. Civil Engineers, Part 2, 91, pp. 561-576.

LAUNDER, B.E. and SPALDING, D.B., (1974) 'The numerical computation of turbulent flows', Comput. Methods Appl. Mech. Eng., 3, pp. 269-289.

LI, C.W., (1990) 'Advection simulation by minimax characteristics method', J. Hydraul. Eng. ASCE, 9, 1138-1144.

LI, C.W. and YIP, K.W., (1999), 'Residence time in semi-enclosed water bodies' Civil and Environmental Engineering Conference, AIT.

LI, C.W. and YU, T.S. (1996) 'Numerical investigation of turbulent shallow recirculating flow by a quasi-three-dimensional  $k$ - $\epsilon$  model', Int. J. Numer. Methods Fluids, 23, 485-501.

LI, C.W. & ZHANG, Y.F., (1998) 'Simulation of free surface recirculating flows in semi-enclosed water bodies by a  $k$ - $\omega$  model', Applied Mathematical Modelling, 22, 153-164.

LI, C.W., ZHANG, Y.F., and YU, T.S., (1996) 'A quasi-three-dimensional  $k$ - $\omega$  model for shallow recirculating flows in an open channel', The Second International Conference on Hydrodynamics, pp. 977-982.

SANDFORD, L.P., BOICOURT, W.C. and RIVES, S.R., (1991) 'Model for estimating tidal flushing of small embayments', J. Waterway, Port, Coastal & Ocean Engrg., pp. 635-654.

VAN SCHIJNDEL, S.A.H. and KRANENBURG, C., (1998), 'Reducing the siltation of a river harbour', J. Hydr. Res., vol. 36, pp.803-814.

WILCOX, 1993, *Turbulence Modelling for CFD*. DCW Industries, Inc.

ZHU, L. and LI, C.W. (1993) 'Error study on numerical approximation of radiation boundary condition for one-dimensional wave equation', Communications in Numerical Methods in Engineering, 9, 475-482.

## List of Symbols

$b$	= return flow factor (fraction of water leaving during ebb that returns during flood)
$\bar{c}$	= average concentration of a solute in the water body
$c$	= average concentration at the entrance of the water body
$c_a$	= background concentration.
$g$	= acceleration due to gravity
$h_k$	= thickness of layer $k$
$k$	= turbulence kinetic energy of layer $k$
$n$	= Manning's coefficient
$q$	= average volume flux leaving the water body
$q$	= longitudinal flow rate in layer $k$
$q$	= transverse flow rate in layer $k$
$s$	= energy slope
$u_*$	= bottom shear velocity
$x$	= longitudinal co-ordinate direction
$y$	= transverse co-ordinate direction
$z$	= vertical co-ordinate direction
$A$	= sectional area of the harbour entrance
$A_s$	= surface area of the water body
$C_0$	= initial spatially averaged concentration within the harbour
$C_i$	= final spatially averaged concentration within the harbour after $i$ tidal cycles
$C_k$	= solute concentration in layer $k$
$C_\mu$	= 0.09
$C_{1\epsilon}$	= 1.44
$C_{2\epsilon}$	= 1.92
$E$	= average per cycle exchange coefficient
$H$	= total water depth

$N$  = total number of layers  
 $P$  = tidal prism =  $AR$   
 $Q$  =  $P/T$   
 $R$  = tidal range  
 $T$  = tidal period.  
 $\bar{U}$  = mean velocity in x direction  
 $U_k$  = longitudinal velocity in layer k  
 $V$  = volume of the water body,  
 $V_k$  = transverse velocity in layer k  
 $\varepsilon$  = turbulence dissipation of layer k  
 $\eta$  = free surface elevation  
 $\kappa$  = von Karman's constant

$\sigma_t$  = turbulent Schmidt number  
 $\sigma_k$  = 1.0  
 $\sigma_\varepsilon$  = 1.3  
 $\tau$  =  $q/V$  = residence time  
 $\tau_{bx}, \tau_{by}$  = bottom stress in x & y direction respectively  
 $\tau_{sx}, \tau_{sy}$  = surface stress in x & y direction respectively  
 $u_a$  = velocity in the river  
 $\nu_k$  = eddy viscosity in layer k  
 $\Delta x, \Delta y, \Delta z$  = grid size in x, y, z directions respectively  
 $\Phi_k$  =  $h_k C_k$